Virial expansion of attractively interacting Fermi gases in one, two, and three dimensions, up to fifth order

Y. Hou◉ and J. E. Drut

Department of Physics and Astronomy, University of North Carolina, Chapel Hill, North Carolina 27599, USA

The virial expansion characterizes the high-temperature approach to the quantum-classical crossover in any quantum many-body system. Here, we calculate the virial coefficients up to the fifth order of Fermi gases in one, two, and three dimensions, with attractive contact interactions, as relevant for a variety of applications in atomic and nuclear physics. To that end, we discretize the imaginary-time direction and calculate the relevant canonical partition functions. In coarse discretizations, we obtain analytic results featuring relationships between the interaction-induced changes Δb_3, Δb_4, and Δb_5 as functions of Δb_2, the latter being exactly known in many cases by virtue of the Beth-Uhlenbeck formula. Using automated-algebra methods, we push our calculations to progressively finer discretizations and extrapolate to the continuous-time limit. We find excellent agreement for Δb_3 with previous calculations in all dimensions and we formulate predictions for Δb_4 and Δb_5 in one and two dimensions. We also provide, for a range of couplings, the subspace contributions Δb_{31}, Δb_{22}, Δb_{41}, and Δb_{32}, which determine the equation of state and static response of polarized systems at high temperature. As a performance check, we compare the density equation of state and Tan contact with quantum Monte Carlo calculations, diagrammatic approaches, and experimental data where available. Finally, we apply Padé and Padé-Borel resummation methods to extend the usefulness of the virial coefficients to approach and in some cases go beyond the unit-fugacity point.

I. INTRODUCTION

The thermodynamics of interacting fermions at finite density is largely (though not only) controlled by the value of the temperature T relative to the Fermi energy scale ϵ_F or alternatively the chemical potential μ. For systems with attractive interactions, the regime $\beta\mu \gg 1$, where $\beta = 1/(k_BT)$, often contains the onset of a superfluid or superconducting transition, while in the region $\beta\mu \simeq 0$ a crossover regime between quantum and classical physics takes place. When $z = e^{\beta\mu} \ll 1$, systems are in a dilute, high-temperature regime whose thermodynamics is captured by the virial expansion, i.e., an expansion in powers of z. Such an expansion encodes, at a given order n, the physics of the n-body problem in the form of virial coefficients. The simplest form of the virial expansion is that of the pressure (which is naturally inherited by the density and the compressibility), with corresponding coefficients usually denoted by b_n.

The applications of the virial expansion in quantum many-body physics have mushroomed in recent years with the equally widespread multiplication of ultracold-atom laboratories around the world (see, e.g., Refs. [1–5]). Indeed, as the density is among the easiest thermodynamic observables to determine experimentally [6–9], the virial expansion has served as a natural nonperturbative anchor for the results of a variety of theoretical approaches to quantum many-body physics (see Ref. [10] for a review). Applications of the expansion in nuclear physics have also been explored, although to a lesser extent, in the context of finite-temperature neutron matter [11–13].

In the recent work of Ref. [14], a "semiclassical" lattice approximation to the calculation of b_n was put forward and applied at leading order for the interaction-induced changes Δb_3 and Δb_4, of spin-1/2 Fermi gases in arbitrary spatial dimensions. The results were compared with quantum Monte Carlo (QMC) calculations in one and two dimensions as well as diagrammatic approaches in two dimensions. Notably, while that approximation corresponds to a maximally coarse Trotter-Suzuki factorization of the imaginary-time evolution operator, the answers were in good quantitative agreement. Reference [15] carried out the approximation one order further and up to Δb_7, with similar results when comparing with previous calculations (where available). Tests of the coarse approximation for Δb_3 and Δb_4 in a harmonic trapping potential were also obtained, in Ref. [16], which showed remarkable qualitative and semiquantitative agreement with prior calculations as a function of the trap frequency. Finally, Ref. [17] used the leading-order approximation to study the thermodynamics of rotating matter.

Encouraged by such a positive experience, here we take the calculation up to Δb_5 by refining the factorization as much as possible for each virial coefficient. We extend our work to one and two dimensions, focus still on attractive contact interactions, and present applications to the equation of state and Tan contact. For completeness, we also discuss aspects of the three-dimensional (3D) system here that we did not discuss in our previous work [18], namely, the isothermal compressibility. In all cases, we present the decomposition of Δb_n in terms of its subspace contributions, namely, Δb_{31} and Δb_{22} for Δb_4, and Δb_{41} and Δb_{32} for Δb_5. These subspace

contributions are not often discussed, but they are important: they determine the thermodynamics (energy, entropy, density, static response, and so on) of the polarized systems. Furthermore, as we will see, Δb_{mj} displays simpler and more systematic behavior than Δb_n as a function of the order in the expansion and the coupling strength. Finally, we take a step further and analyze the virial coefficients using resummation techniques, namely, the Padé and Borel-Padé methods, which substantially extend the applicability (in a practical sense) of the virial expansion in all the cases we studied.

The remainder of this paper is organized as follows. Section II presents the Hamiltonian we focus on along with the formal elements of the virial expansion, and explains the basics of our approach, which is based on the discretization of imaginary time by a Trotter-Suzuki factorization of the Boltzmann weight. Section III presents our analytic formulas for canonical partition functions in Sec. III A and virial coefficients for arbitrary spatial dimension in Sec. III B. In Sec. IV, we show our results from extrapolating to the continuous-time limit. Specifically, Secs. IV A–IV F show our results for virial coefficients and corresponding applications in one, two, and three dimensions. As a way to extend the application of the virial expansion, we use Padé and Padé-Borel resummation techniques, which we comment on in Sec. IV G. Finally, we summarize and conclude in Sec. V.

II. HAMILTONIAN, VIRIAL EXPANSION, AND METHOD

The simplest interacting effective theory one can write for nonrelativistic spin-1/2 fermions in d spatial dimensions has a Hamiltonian given by $\hat{H} = \hat{T} + \hat{V}$, where

$$\hat{T} = \sum_{s=\uparrow,\downarrow} \int d^d x \, \hat{\psi}_s^\dagger(\mathbf{x}) \left(-\frac{\hbar^2 \nabla^2}{2m} \right) \hat{\psi}_s(\mathbf{x}), \qquad (1)$$

and

$$\hat{V} = -g_d \int d^d x \, \hat{n}_\uparrow(\mathbf{x}) \hat{n}_\downarrow(\mathbf{x}), \qquad (2)$$

where the field operators $\hat{\psi}_s$, $\hat{\psi}_s^\dagger$ are fermionic fields for particles of spin $s = \uparrow, \downarrow$, and $\hat{n}_s(\mathbf{x})$ are the coordinate-space densities. In the remainder of this work, we take $\hbar = k_B = m = 1$. To regularize the interaction, we put the Hamiltonian on a spatial lattice of spacing ℓ, whose calibration is determined by our renormalization condition, as explained below.

As mentioned above, the virial expansion is an expansion around the dilute limit $z \to 0$, where $z = e^{\beta\mu}$ is the fugacity, β is the inverse temperature, and μ the chemical potential coupled to the total particle number operator $\hat{N}$. The coefficient accompanying the nth power of z in the expansion of the grand-canonical potential Ω is the virial coefficient b_n:

$$-\beta\Omega = \ln \mathcal{Z} = Q_1 \sum_{n=1}^{\infty} b_n z^n, \qquad (3)$$

where

$$\mathcal{Z} = \mathrm{tr}[e^{-\beta(\hat{H} - \mu\hat{N})}] = \sum_{N=0}^{\infty} z^N Q_N \qquad (4)$$

is the grand-canonical partition function. Q_N is the N-body partition function, $b_1 = 1$, and the higher-order coefficients are given by

$$Q_1 b_2 = Q_2 - \frac{Q_1^2}{2!}, \qquad (5)$$

$$Q_1 b_3 = Q_3 - b_2 Q_1^2 - \frac{Q_1^3}{3!}, \qquad (6)$$

$$Q_1 b_4 = Q_4 - \left(b_3 + \frac{b_2^2}{2} \right) Q_1^2 - b_2 \frac{Q_1^3}{2!} - \frac{Q_1^4}{4!}, \qquad (7)$$

$$Q_1 b_5 = Q_5 - (b_4 + b_2 b_3) Q_1^2 - (b_2^2 + b_3) \frac{Q_1^3}{2} - b_2 \frac{Q_1^4}{3!} - \frac{Q_1^5}{5!}, \qquad (8)$$

etc. The noninteracting virial coefficients for nonrelativistic fermions in d spatial dimensions are $b_n^{(0)} = (-1)^{n+1} n^{-(d+2)/2}$.

The highest power of Q_1 does not involve any virial coefficients and therefore always disappears in the interaction change Δb_n:

$$Q_1 \Delta b_2 = \Delta Q_2, \qquad (9)$$

$$Q_1 \Delta b_3 = \Delta Q_3 - Q_1^2 \Delta b_2, \qquad (10)$$

$$Q_1 \Delta b_4 = \Delta Q_4 - \Delta\left(b_3 + \frac{b_2^2}{2} \right) Q_1^2 - \frac{\Delta b_2}{2} Q_1^3, \qquad (11)$$

$$Q_1 \Delta b_5 = \Delta Q_5 - \Delta(b_4 + b_2 b_3) Q_1^2$$
$$- \frac{1}{2} \Delta(b_2^2 + b_3) Q_1^3 - \frac{\Delta b_2}{3!} Q_1^4. \qquad (12)$$

Furthermore, in terms of the partition functions Q_{MN} of M particles of one type and N of the other type, we have

$$\Delta Q_2 = \Delta Q_{11}, \qquad (13)$$

$$\Delta Q_3 = 2\Delta Q_{21}, \qquad (14)$$

$$\Delta Q_4 = 2\Delta Q_{31} + \Delta Q_{22}, \qquad (15)$$

$$\Delta Q_5 = 2\Delta Q_{32} + 2\Delta Q_{41}. \qquad (16)$$

Therefore, the main complexity in the calculations presented below is in computing the few ΔQ_{MN} shown above within the Trotter-Suzuki factorization of the imaginary-time evolution operator, which we discuss next.

Trotter-Suzuki factorization

To carry out our calculations, we factorize the imaginary-time evolution operator in the style of Trotter-Suzuki, such that

$$e^{-\beta(\hat{T} + \hat{V})} \simeq (e^{-\beta\hat{T}/k} e^{-\beta\hat{V}/k})^k, \qquad (17)$$

where setting $k = 1$ defines the coarsest possible discretization. In this work we take $k \gg 1$ and as far as possible. For low k, however, we carry out analytic calculations leading to explicit formulas which are useful for cross-checks across

dimensions, as they feature the spatial dimension d as a parameter.

For $k = 1$ we have

$$e^{-\beta(\hat{T}+\hat{V})} \simeq e^{-\beta\hat{T}} e^{-\beta\hat{V}}, \tag{18}$$

which is equivalent to neglecting $[\hat{T}, \hat{V}]$ and higher-order commutators; for that reason we have called this a semiclassical expansion in previous works. In all cases of interest here, the expressions will appear inside a trace, such that the error is pushed to $O(1/k^2)$. Indeed, as far as the trace is concerned, Eq. (18) is equivalent to the more accurate, symmetric decomposition

$$e^{-\beta(\hat{T}+\hat{V})} \simeq (e^{-\beta\hat{T}/(2k)} e^{-\beta\hat{V}/k} e^{-\beta\hat{T}/(2k)})^k, \tag{19}$$

whose error is $O(1/k^2)$.

III. ANALYTIC RESULTS

In this section we present our main analytic results. In Sec. III A we present partition functions for $k = 2$ and in Sec. III B virial coefficients up to the fifth order for $k = 1$ and $k = 2$. In all cases the results feature the spatial dimension d as a variable. Our analytic results are shown as examples and cross-checks for the method, and for future reference.

A. Canonical partition functions for $k = 2$

As the simplest nontrivial example, we work out in detail Q_{11} which determines b_2 and therefore plays a central role in our method. For $k = 2$, the calculation begins as follows:

$$Q_{11} = \sum_{\mathbf{p}_1\mathbf{p}_2} \langle \mathbf{p}_1\mathbf{p}_2 | e^{-\frac{\beta\hat{T}}{2}} e^{-\frac{\beta\hat{V}}{2}} e^{-\frac{\beta\hat{T}}{2}} e^{-\frac{\beta\hat{V}}{2}} | \mathbf{p}_1\mathbf{p}_2 \rangle$$

$$= \sum_{\mathbf{p}_1\mathbf{p}_2\mathbf{p}_3\mathbf{p}_4} e^{-\beta(\mathbf{p}_1^2+\mathbf{p}_2^2)/4m} e^{-\beta(\mathbf{p}_3^2+\mathbf{p}_4^2)/4m}$$

$$\times \langle \mathbf{p}_1\mathbf{p}_2 | e^{-\beta\hat{V}/2} | \mathbf{p}_3\mathbf{p}_4 \rangle \langle \mathbf{p}_3\mathbf{p}_4 | e^{-\beta\hat{V}/2} | \mathbf{p}_1\mathbf{p}_2 \rangle. \tag{20}$$

The next step is to insert a coordinate-space completeness relation and use the following identity:

$$e^{-\beta\hat{V}/2} | \mathbf{x}_1\mathbf{x}_2 \rangle = \prod_{\mathbf{z}} (1 + C\hat{n}_\uparrow(\mathbf{z})\hat{n}_\downarrow(\mathbf{z})) | \mathbf{x}_1\mathbf{x}_2 \rangle$$

$$= | \mathbf{x}_1\mathbf{x}_2 \rangle + C \sum_{\mathbf{z}} \delta_{\mathbf{x}_1,\mathbf{z}} \delta_{\mathbf{x}_2,\mathbf{z}} | \mathbf{x}_1\mathbf{x}_2 \rangle$$

$$= [1 + C\delta_{\mathbf{x}_1,\mathbf{x}_2}] | \mathbf{x}_1\mathbf{x}_2 \rangle, \tag{21}$$

where $C = (e^{\beta g_d/2} - 1)\ell^d$ and we used the fermionic relation $\hat{n}_s^2 = \hat{n}_s$. Note that the series in powers of C terminates at linear order for this particular state in which there is only one particle for one of the species (regardless of how many particles of the other species are present). The C-independent term yields the noninteracting result, such that

$$\Delta Q_{11} = \sum_{\mathbf{PP'XX'}} e^{-\beta(\mathbf{P}^2+\mathbf{P'}^2)/4m} \langle \mathbf{P}|\mathbf{X}\rangle \langle \mathbf{X}|\mathbf{P'}\rangle \langle \mathbf{P'}|\mathbf{X'}\rangle \langle \mathbf{X'}|\mathbf{P}\rangle$$

$$\times [C(\delta_{\mathbf{x}_1,\mathbf{x}_2} + \delta_{\mathbf{x'}_1,\mathbf{x'}_2}) + C^2(\delta_{\mathbf{x}_1,\mathbf{x}_2}\delta_{\mathbf{x'}_1,\mathbf{x'}_2})], \tag{22}$$

where $\mathbf{P}$ is the shorthand for the set of momentum variables $\mathbf{p}_1$ and $\mathbf{p}_2$ and $\mathbf{P}^2 = \mathbf{p}_1^2 + \mathbf{p}_2^2$, and similarly for $\mathbf{P'}$, $\mathbf{X}$, $\mathbf{X'}$.

Using a plane-wave basis, $|\langle \mathbf{x}_1\mathbf{x}_2|\mathbf{p}_1\mathbf{p}_2\rangle|^2 = 1/V^2$, where $V = L^d$ in d spatial dimensions and L is the linear extent of the system, and we then find

$$\Delta Q_{11} = C \frac{f_1}{V} + C^2 \frac{f_2}{V^2}, \tag{23}$$

where $f_1 = 2Q_{10}^2$, with

$$Q_{10} = \sum_{\mathbf{p}_1} e^{-\beta p_1^2/2m}, \tag{24}$$

and

$$f_2 = \sum_{\mathbf{p}_1\mathbf{p}_2\mathbf{p}_3} e^{-\beta[\mathbf{p}_1^2+\mathbf{p}_2^2+\mathbf{p}_3^2+(\mathbf{p}_1+\mathbf{p}_2-\mathbf{p}_3)^2]/4m}. \tag{25}$$

In the continuum limit, in d spatial dimensions,

$$Q_{10} = \left(\frac{L}{\lambda_T}\right)^d, \tag{26}$$

$$f_1 = 2\left(\frac{L}{\lambda_T}\right)^{2d}, \qquad f_2 = \left(\frac{L}{\lambda_T}\right)^{3d} 2^{\frac{d}{2}}, \tag{27}$$

where $\lambda_T = \sqrt{2\pi\beta}$ is the thermal wavelength.

Thus,

$$\Delta Q_{11} = 2\left(\frac{L}{\lambda_T}\right)^d \left[\frac{C}{\lambda_T^d} + 2^{\frac{d}{2}-1}\left(\frac{C}{\lambda_T^d}\right)^2\right], \tag{28}$$

such that

$$\Delta b_2 = \frac{\Delta Q_{11}}{Q_1} = \frac{C}{\lambda_T^d} + 2^{\frac{d}{2}-1}\left(\frac{C}{\lambda_T^d}\right)^2, \tag{29}$$

where we have used $Q_1 = 2Q_{10}$.

As explained in the Introduction, only a few canonical partition functions enter in Δb_n. For $n = 3, 4, 5$ all we need is ΔQ_{21}, ΔQ_{31}, ΔQ_{22}, ΔQ_{41}, and ΔQ_{32}. Of these, the last two are the most mathematically demanding. Below we present a sample of our analytic results for $k = 2$ for selected partition functions (excluding ΔQ_{41} and ΔQ_{32}) in the continuum limit.

Calculating Δb_3 requires Δb_2 and the following result:

$$\frac{2\Delta Q_{21}}{Q_1} = \frac{C}{\lambda_T^d} \left[-2^{1-\frac{d}{2}} + \left(\frac{L}{\lambda_T}\right)^d\right]$$

$$+ \left(\frac{C}{\lambda_T^d}\right)^2 \left[\left(1 - \frac{2^{d+1}}{5^{\frac{d}{2}}}\right) + 2^{\frac{d}{2}}\left(\frac{L}{\lambda_T}\right)^d\right]. \tag{30}$$

Both of the contributions displaying explicit dependence on L/λ_T will cancel out in the final expression for Δb_3, giving a volume-independent result.

Calculating Δb_4 requires Δb_2, Δb_3, and the following two results:

$$\frac{2\Delta Q_{31}}{Q_1} = \frac{C}{\lambda_T^d}\left[\frac{2}{3^{\frac{d}{2}}} - \frac{3}{2^{\frac{d}{2}}}\left(\frac{L}{\lambda_T}\right)^d + \left(\frac{L}{\lambda_T}\right)^{2d}\right] + \left(\frac{C}{\lambda_T^d}\right)^2\left[\frac{1}{3^{\frac{d}{2}}} + \left(\frac{1}{2} - \frac{2^{d+1}}{5^{\frac{d}{2}}}\right)\left(\frac{L}{\lambda_T}\right)^d + \frac{1}{2^{1-\frac{d}{2}}}\left(\frac{L}{\lambda_T}\right)^{2d}\right], \tag{31}$$

$$\frac{\Delta Q_{22}}{Q_1} = \frac{C}{\lambda_T^d}\left[2^{-d} - 2^{1-\frac{d}{2}}\left(\frac{L}{\lambda_T}\right)^d + \left(\frac{L}{\lambda_T}\right)^{2d}\right] + \left(\frac{C}{\lambda_T^d}\right)^2\left[\left(2^{-d-1} + \frac{2}{3^{\frac{d}{2}}} - \frac{3}{2^{\frac{d}{2}}}\right) + 2\left(1 - \frac{2^d}{5^{\frac{d}{2}}}\right)\left(\frac{L}{\lambda_T}\right)^d + 2^{\frac{d}{2}-1}\left(\frac{L}{\lambda_T}\right)^{2d}\right]$$

$$+ \left(\frac{C}{\lambda_T^d}\right)^3\left[\left(1 + 2^{1-\frac{d}{2}} - \frac{2^{2+d}}{5^{\frac{d}{2}}}\right) + 2^{\frac{d}{2}}\left(\frac{L}{\lambda_T}\right)^d\right] + \left(\frac{C}{\lambda_T^d}\right)^4\left[\left(\frac{3}{4} - \frac{2^d}{3^{\frac{d}{2}}}\right) + 2^{-2+d}\left(\frac{L}{\lambda_T}\right)^d\right]. \tag{32}$$

As mentioned above, also in this case, the explicit dependence on L/λ_T will be canceled in the final expression for Δb_4. Only the volume-independent terms will remain.

In the next section, we use the above expressions to assemble the calculation of Δb_3 and Δb_4, using Eqs. (9)–(16) at $k = 2$. We will, in fact, go beyond the above expressions and present results for Δb_5 as well, and extend the whole analysis to $k = 3, 4$ and extrapolate to the continuous-time limit. As the equations for $k \geqslant 3$ are much too long to be displayed in the present format in a useful manner, we have written a PYTHON code that evaluates our formulas for $k = 1, 2, 3, 4$, available as part of our Supplemental Material [19]. (Note, however, that beyond the analytic results presented here, where the spatial dimension d appears explicitly, we do not show continuous cross-dimensional results for the virial coefficients in this work but rather focus on one, two, and three dimensions. The Supplemental Material contains the numerical values of the virial coefficients in one, two, and three dimensions, after extrapolation to the large-k limit.)

B. Virial coefficients: Analytic results at $k = 1$ and $k = 2$ across dimensions

Previous work [14,15] calculated the virial coefficients at $k = 1$, which yields, for a fermionic two-species system with

a contact interaction, in d spatial dimensions,

$$\Delta b_3 = -2^{1-\frac{d}{2}}\Delta b_2, \tag{33}$$

$$\Delta b_4 = 2(3^{-\frac{d}{2}} + 2^{-d-1})\Delta b_2 + 2^{1-\frac{d}{2}}(2^{-\frac{d}{2}-1} - 1)(\Delta b_2)^2, \tag{34}$$

where we have corrected the coefficient of $(\Delta b_2)^2$ relative to Ref. [14]. Also at $k = 1$, but going beyond the work of Ref. [14], Ref. [15] found

$$\Delta b_5 = -(2^{-d} + 6^{-\frac{d}{2}})\Delta b_2 + 4(2^{-d} + 3^{-\frac{d}{2}} - 7^{-\frac{d}{2}})(\Delta b_2)^2, \tag{35}$$

which we show here for completeness as we will calculate Δb_5 at higher k.

As part of our main results, we have extended the above calculations to higher k for Δb_3, Δb_4, and Δb_5. For $k = 2$ one can write explicit formulas that easily fit on a sheet of paper:

$$\Delta b_2 = \tilde{C} + 2^{\frac{d}{2}-1}\tilde{C}^2, \tag{36}$$

$$\Delta b_3 = -2^{1-\frac{d}{2}}\tilde{C} + \left(1 - \frac{2^{1+d}}{5^{\frac{d}{2}}}\right)\tilde{C}^2, \tag{37}$$

$$\Delta b_4 = 2(3^{-\frac{d}{2}} + 2^{-d-1})\tilde{C} + \left(3^{1-\frac{d}{2}} + 2^{-d-1} - \frac{3}{2^{\frac{d}{2}}}\right)\tilde{C}^2 + \left(1 + 2^{1-\frac{d}{2}} - \frac{2^{d+2}}{5^{\frac{d}{2}}}\right)\tilde{C}^3 + \left(\frac{3}{4} - \frac{2^d}{3^{\frac{d}{2}}}\right)\tilde{C}^4, \tag{38}$$

$$\Delta b_5 = -\left(2^{1-d} + \frac{2^{1-\frac{d}{2}}}{3^{\frac{d}{2}}}\right)\tilde{C} + \left(\frac{7}{2^d} - \frac{2^{1+d}}{3^{\frac{3d}{2}}} + \frac{7}{3^{\frac{d}{2}}} - \frac{2}{7^{\frac{d}{2}}} - \frac{2^{1+d}}{11^{\frac{d}{2}}} - 3 \times \frac{2^{1+d}}{19^{\frac{d}{2}}}\right)\tilde{C}^2$$

$$+ \left[2^{1-d} - 2^{1-\frac{d}{2}} + 4 \times 3^{1-\frac{d}{2}} - 2^{\frac{d}{2}+2}\left(\frac{2}{3^d} + 5^{-\frac{d}{2}} - 7^{-\frac{d}{2}}\right)\right]\tilde{C}^3 + \left(1 + 2^{2-\frac{d}{2}} - 2^{1+d}3^{1-d} - 3 \times \frac{2^{1+d}}{5^{\frac{d}{2}}}\right)$$

$$- \frac{4^d}{3^d 5^{\frac{d}{2}}} + \frac{3^{1-\frac{d}{2}}4^d}{7^{\frac{d}{2}}} + 3 \times \frac{2^{1+2d}}{29^{\frac{d}{2}}}\right)\tilde{C}^4, \tag{39}$$

where $\tilde{C} = (e^{\beta g_d/2} - 1)\ell^d/\lambda_T^d$. Although we used these $k = 2$ results in a previous work [15], we did not include the above formulas explicitly.

Note that, while the above expressions resemble truncated power series in $\tilde{C}$, they actually display the full answer for $k = 2$. Furthermore, we note that as in the $k = 1$ case, in the

$k = 2$ case Δb_2 is always positive and Δb_3 is always negative, for positive $\tilde{C}$ in $d = 1, 2, 3$. The behavior of Δb_4 and Δb_5, however, is less obvious, which is at least in part because they are the result of competing subspace contributions (see Ref. [18] and our discussion below). Solving for $\tilde{C}$ in terms of Δb_2 at $k = 2$, we find

$$\tilde{C} = 2^{-\frac{d}{2}}(\sqrt{1 + 2^{\frac{d}{2}+1}\Delta b_2} - 1), \qquad (40)$$

where we have chosen the solution that yields a real and positive value for $\tilde{C}$, which corresponds to attractive interactions and thus positive Δb_2. Using that result yields Δb_3, Δb_4, and Δb_5 in terms of Δb_2. In the sections that follow we use the above formulas and their generalizations to $k = 3$ and beyond to display the behavior of virial coefficients as k is increased and compare those results with the extrapolations to the large-k limit.

IV. EXTRAPOLATED RESULTS

In this section we focus on the physically relevant cases of one-dimensional (1D), two-dimensional (2D), and 3D attractive Fermi gases, extrapolating to the large-k (i.e., continuous-time) limit. Specifically, we calculated the interaction-induced changes in the virial coefficients Δb_3 up to $k = 21$, Δb_4 up to $k = 12$, and Δb_5 up to $k = 9$, and based on those results we extrapolated to $k \to \infty$ using the techniques discussed in Ref. [18].

In each spatial dimension, we discuss applications centered around measurable quantities such as the density equation of state, Tan contact, and the isothermal compressibility. The applicability and usefulness of the calculated coefficients extends well beyond those observables, however, as the Δb_n also determine the high-temperature behavior of a broad suite of thermodynamic quantities such as the energy, entropy, pressure, magnetic susceptibility, etc. Furthermore, we focus largely on unpolarized systems (the exceptions being the density equation of state in one and three dimensions at unitarity), but provide the subspace decomposition of Δb_4 and Δb_5, which extend the applicability of our results to the polarized-system version of the aforementioned thermodynamic quantities.

A. Virial coefficients in one dimension

To calculate the virial coefficients of attractively interacting fermions in one dimension we used the technique described above combined with the exact Beth-Uhlenbeck result [20,21]

$$\Delta b_2^{\text{1D,exact}} = -\frac{1}{2\sqrt{2}} + \frac{e^{\lambda_1^2/4}}{2\sqrt{2}}[1 + \text{erf}(\lambda_1/2)]. \qquad (41)$$

This equation, together with Eq. (40) (and its counterparts at higher k), allows us to obtain $\tilde{C}$ as a function of the dimensionless physical coupling $\lambda_1 = 2\sqrt{\beta}/a_0$, where a_0 is the 1D scattering length.

The results of our 1D calculations are shown in Fig. 1 and are in excellent agreement with the QMC data of Ref. [14] for Δb_3 and Δb_4. For the latter, the QMC calculations are very
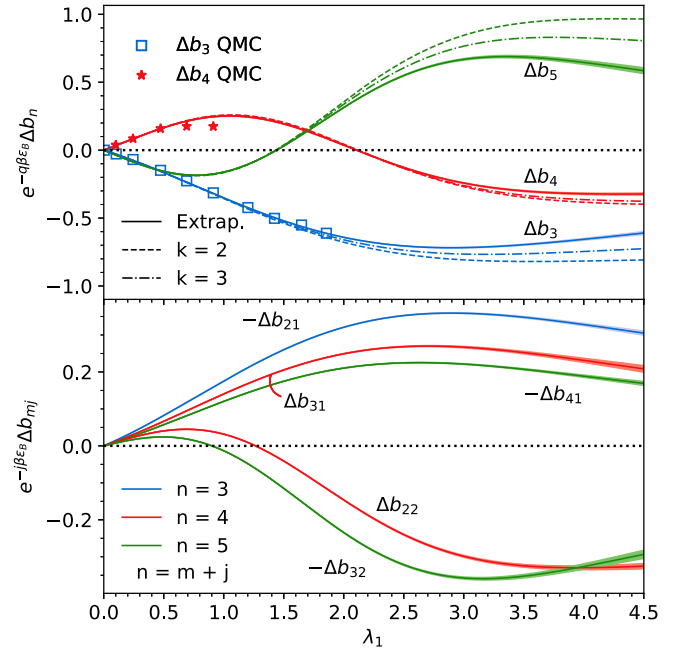
FIG. 1. Top: Virial coefficients Δb_n for $n = 3\text{–}5$ for the 1D attractive Fermi gas as a function of the dimensionless coupling λ_1. To fit the scale, the Δb_ns are scaled by $\exp(-q\beta\epsilon_b)$, where q is the maximum number of spin-↑↓ pairs. The $k = 2$ results are shown as dashed lines, $k = 3$ as dash-dotted lines, and the $k \to \infty$ extrapolation with solid lines. Results for Δb_3 appear in blue, Δb_4 in red, and Δb_5 in green (as labeled). Blue squares and red stars show the QMC results for Δb_3 and Δb_4, respectively, from Ref. [14]. Bottom: Subspace contributions Δb_{mj} as functions of the coupling strength, scaled by $\exp(-j\beta\epsilon_b)$. Our results are shown as labeled error bands, color coded as in the top plot by $n = m + j$: blue for $-\Delta b_{21}$, red for Δb_{31} and Δb_{22}, and green for $-\Delta b_{41}$ and $-\Delta b_{32}$. Specific cases are inverted in sign for clarity and to avoid overlaps.

limited and stop beyond $\lambda_1 \simeq 1.0$ (where the QMC method begins to break down), whereas our present results go well beyond that region. Because a two-body bound state forms in this system as soon as the interaction is turned on, the virial coefficients will tend to grow exponentially with the binding energy (as is evident at second order from the Beth-Uhlenbeck formula). To capture that behavior, we scaled our virial coefficients by the inverse Boltzmann weight $\exp(-q\beta\epsilon_B)$ of the available particle pairs q (i.e., $q = 1$ for Δb_3 and $q = 2$ for Δb_4 and Δb_5), where $\epsilon_B = 1/a_0^2$ is the binding energy of the two-body system. The resulting mild behavior at strong coupling shows that indeed the scaling factor captures the shape of Δb_n as the coupling is increased. Beyond that leading contribution, however, Δb_3 is controlled by the atom-dimer scattering properties, just as Δb_4 is controlled by dimer-dimer properties, and so on. In all the dimensions explored here, we found that Δb_3 is of constant sign, whereas Δb_4 and Δb_5 change sign at strong enough coupling, as a result of the competition between positive and negative contributions coming from the fixed-polarization subspaces Δb_{mj}.

The Δb_{mj} are shown in the bottom panel of Fig. 1. There is naturally only one subspace contributing at third order:

$\Delta b_3 = 2\Delta b_{21}$. However, $\Delta b_4 = \Delta b_{22} + 2\Delta b_{31}$ and $\Delta b_5 = 2\Delta b_{32} + 2\Delta b_{41}$. Furthermore, in each of the latter, the subspace terms enter with similar magnitudes but opposing signs, and thus compete to determine the sign and size of Δb_n. It is hard to miss that $|\Delta b_{m1}|$ follows essentially the same trend as a function of the coupling across all m, and that trend becomes increasingly suppressed for increasing m. A similar observation applies to $|\Delta b_{m2}|$. The suppression with increased polarization is easy to understand: at large m both $|\Delta b_{m1}|$ and $|\Delta b_{m2}|$ must approach the noninteracting values (i.e., zero) as the majority of the particles do not interact due to Pauli blocking.

B. Applications in one dimension

1. Density equation of state at finite polarization

In the virial expansion, the density equation of state of a polarized system becomes a double series expansion in powers of the fugacity of each spin $z_s = \exp(\beta\mu_s)$, $s = \uparrow, \downarrow$. More specifically, the grand thermodynamic potential $\Omega = \Omega_0 + \Delta\Omega$, relative to its noninteracting counterpart Ω_0, becomes

$$-\beta\Delta\Omega = Q_1 \sum_{n=2}^{\infty} \sum_{\substack{m, j > 0 \\ m+j=n}} \Delta b_{mj} z_\uparrow^m z_\downarrow^j, \qquad (42)$$

such that the particle number density for spin-$\uparrow$ is given by

$$\lambda_T^d n_\uparrow = \lambda_T^d n_{\uparrow,0} + 2 \sum_{n=2}^{\infty} \sum_{\substack{m, j > 0 \\ m+j=n}} m \Delta b_{mj} z_\uparrow^m z_\downarrow^j, \qquad (43)$$

where $\lambda_T = \sqrt{2\pi\beta}$ is the thermal wavelength, $\lambda_T^d n_{\uparrow,0} = f_{d/2}(z_\uparrow)$ is the noninteracting value in d dimensions, $f_{d/2}(z) = \mathrm{Li}_{d/2}(-z)$ is the Fermi-Dirac function, and $\mathrm{Li}_s(x)$ is the polylogarithm function. An analogous expression to Eq. (43) holds for $\lambda_T^d n_\downarrow$.

In Fig. 2 we show our estimates for the density equation of state at finite polarization in the virial expansion, for attractively interacting fermions in one dimension. We compare our results with those of Ref. [22] obtained with the complex Langevin method. The fifth-order virial expansion provides a modest improvement over the third and fourth orders. However, for all the available polarizations the agreement with the data is reasonable as long as $\beta\mu$ is sufficiently small. Resummation techniques (see below) like Padé approximants extend that agreement (which, while not perfect, is better than qualitative) with the available data over a wider $\beta\mu$ region.

2. Contact

As elucidated by Tan and others [23–25], in systems with short-range interactions the short-distance and high-frequency behavior of correlation functions is captured by a single quantity called the contact, often denoted by $\mathcal{I}$. The contact also enters celebrated pressure-energy and other exact relations as well as sum rules [26–38] and is therefore a crucial piece of the thermodynamic puzzle that complements conventional quantities. Below, we compare our virial-expansion results for the contact in one dimensions with QMC data.
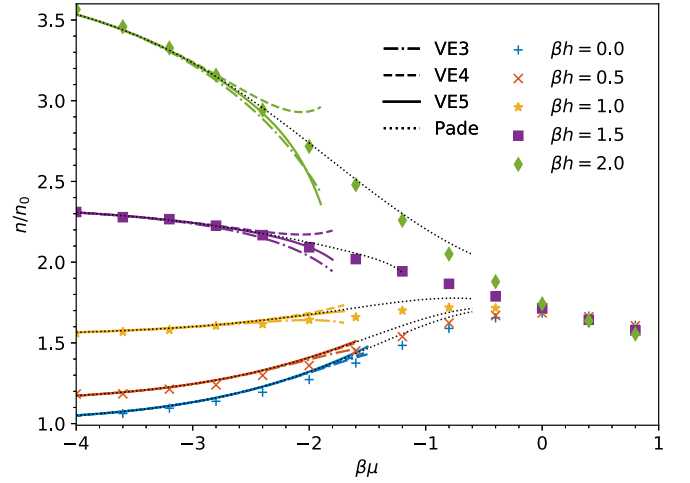

FIG. 2. Density equation of state n of the attractive 1D Fermi gas, shown in units of the noninteracting, unpolarized counterpart n_0 with coupling strength $\lambda_1 = 1.0$, for several values of the chemical potential difference $\beta h = \beta(\mu_\uparrow - \mu_\downarrow)/2$. The colored symbols are complex-Langevin results from Ref. [22] and the colored lines show the virial expansion at various orders: dash-dotted line at third order (VE3), dashed line at fourth order (VE4), and solid line at fifth order (VE5). The black dotted line is the result of the [3/2] Padé resummation (see Sec. IV G). The Padé approximant for $\beta h = 1.5$ contains a pole close to $\beta\mu = -1.2$; the corresponding dotted line is therefore cut off at that value. The limiting value for $\beta\mu \rightarrow -\infty$ is known exactly and is given by $\cosh(\beta h)$.

In one dimension, the contact is given by

$$\mathcal{I} = \frac{2}{\beta} \frac{\partial(\beta\Omega)}{\partial a_0}, \qquad (44)$$

such that its virial expansion becomes

$$\mathcal{I} = \frac{4\pi}{\lambda_T^3} Q_1 \sum_{m=2}^{\infty} c_m z^m, \qquad (45)$$

where $\lambda_T = \sqrt{2\pi\beta}$ and

$$c_m = \sqrt{\frac{\pi}{2}} \lambda_1^2 \frac{\partial \Delta b_m}{\partial \lambda_1}. \qquad (46)$$

The Beth-Uhlenbeck formula yields

$$c_2 = \frac{\lambda_1^2}{4} + \frac{\sqrt{\pi}}{8} e^{\lambda_1^2/4} \lambda_1^3 [1 + \mathrm{erf}(\lambda_1/2)], \qquad (47)$$

as first shown in Ref. [21]. Using the λ_1 dependence of our results for Δb_n, we obtained the virial expansion of $\mathcal{I}$ up to fifth order. In Fig. 3 we show the dimensionless, intensive form of the contact, $\mathcal{I}\pi\beta^2/(2L\lambda_1^2)$ as a function of temperature in the virial expansion. At weak couplings ($\lambda_1 \leqslant 2.0$), the virial expansion shows good agreement with the QMC results of Ref. [21]. However, as the coupling strength increases, the disparity becomes significant, which is not completely unexpected as both methods face challenges in the strong-coupling regime: the radius of convergence of the virial expansion can be very small, such that the expansion ceases to be useful even at very negative $\beta\mu$; on the other hand, the lattice QMC method may suffer from increasing lattice-spacing effects at
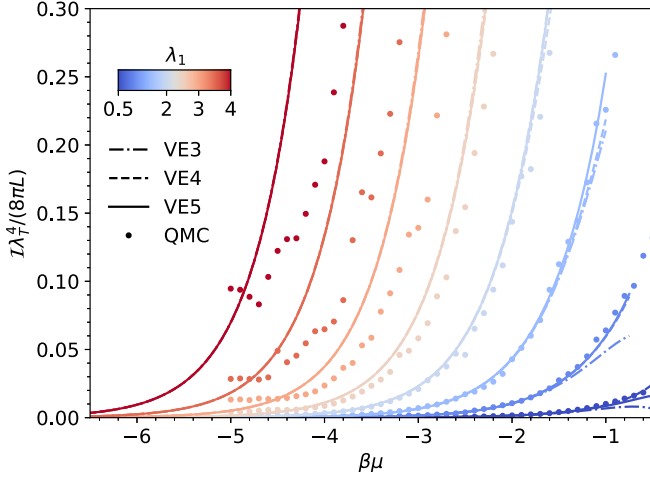
FIG. 3. Tan contact $\mathcal{I}$, in the dimensionless form $\mathcal{I}\pi\beta^2/(2L\lambda_1^2)$, as a function of $\beta\mu$, for the attractive 1D Fermi gas. The dots show the QMC results of Ref. [21] and the curves show the virial expansion at various orders, following the same line style as in Fig. 2. The color encodes the coupling strength from $\lambda_1 = 0.5$ (dark blue) to $\lambda_1 = 4.0$ (dark red) in steps of 0.5. From bottom to top, the curves and data correspond to $\lambda_1 = 0.5, 1.0, 1.5, 2.0, 2.5, 3.0, 3.5,$ and 4.0.

strong coupling, due to the reduced size of the two-body bound state.

C. Virial coefficients in two dimensions

In Fig. 4 we show our results for Δb_n for the 2D Fermi gas with attractive interactions [40]. As in one dimension, we scaled the coefficients by $\exp(-q\beta\epsilon_B)$, where q is the maximum number of available spin-$\uparrow\downarrow$ pairs. To renormalize, we again rely on the exact Beth-Uhlenbeck result [20,39,41–45]

$$\Delta b_2^{2D,\text{exact}} = e^{\lambda_2^2} - \int_0^\infty \frac{dy}{y} \frac{2e^{-\lambda_2^2 y^2}}{\pi^2 + 4\ln^2 y}, \quad (48)$$

to define $\tilde{C}$ as a function of the physical coupling $\lambda_2^2 = \beta\epsilon_B$, where ϵ_B is the binding energy of the two-body system.

At all orders the similarity with one dimension is clear: Δb_3 remains negative for all the couplings studied, whereas Δb_4 and Δb_5 change sign at strong enough coupling as a result of a competition between subspaces Δb_{m1} and Δb_{n2} governed by the number of spin-$\uparrow\downarrow$ pairs available in each subspace. While Δb_4 and Δb_5 are calculated here (thus furnishing a prediction), Δb_3 was calculated in Ref. [39]. The results of the latter are shown in Fig. 4 with blue dots, which agree remarkably well with our answers.

The subspace contributions Δb_{mj} are shown in the bottom panel of Fig. 4 and we again note clear parallels with the 1D case. Specifically, the subspace terms contributing to Δb_4 and Δb_5 enter with similar magnitudes but opposing signs, indicating that the final results for Δb_4 and Δb_5 result from subtle coupling-dependent cancellations. Furthermore, $|\Delta b_{m1}|$ and $|\Delta b_{m2}|$ follow consistent trends as a function of the coupling across all m (with the expected suppression as m is increased). In fact, once the $\exp(-q\beta\epsilon_B)$ factor is included,
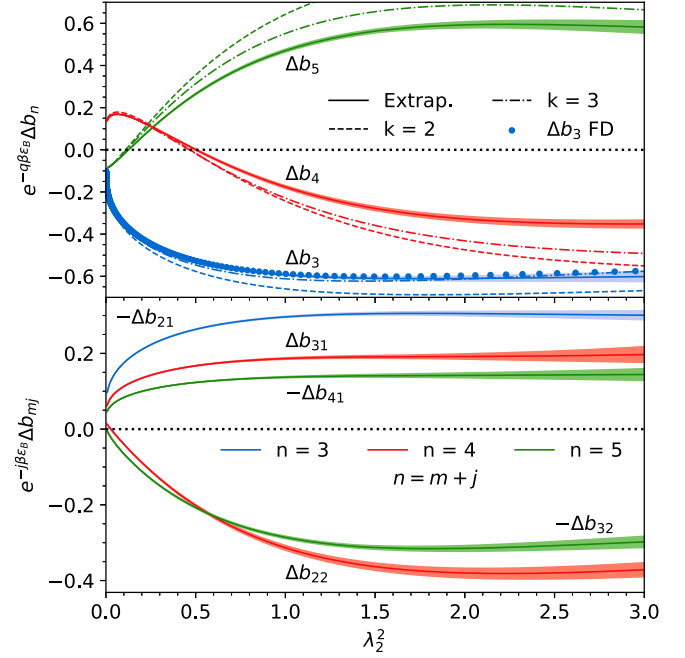

FIG. 4. Top: Virial coefficients Δb_n for $n = 3$–5 for the 2D attractive Fermi gas, as a function of the square of the dimensionless coupling λ_2. To fit the scale, Δb_ns are scaled by $\exp(-q\beta\epsilon_b)$, where q is the maximum number of spin-$\uparrow\downarrow$ pairs, and Δb_{mj}s are scaled by $\exp(-j\beta\epsilon_b)$. The $k = 2$ results are shown as dashed lines, $k = 3$ as dash-dotted lines, and the $k \to \infty$ extrapolation with solid lines. Results for Δb_3 appear in blue, for Δb_4 in red, and for Δb_5 in green (as labeled). The diagrammatic results for Δb_3 from Ref. [39] appear as blue dots. Bottom: Subspace contributions Δb_{mj} as functions of the coupling strength. Our results are shown as labeled error bands, color coded as in the top plot by $n = m + j$: blue for $-\Delta b_{21}$, red for Δb_{31} and Δb_{22}, and green for $-\Delta b_{41}$ and $-\Delta b_{32}$.

$|\Delta b_{m1}|$ and $|\Delta b_{m2}|$ are approximately constant as the coupling is increased.

At weak coupling, on the other hand, the details are elusive in the scale of Fig. 4. There, nonperturbative effects are only visible if shown differently, as we do in Fig. 5, where show that, as functions of Δb_2 all the coefficients tend smoothly to zero as the coupling is weakened. The nonperturbative behavior at weak coupling is completely captured by Δb_2.

D. Applications in two dimensions

1. Density equation of state at zero polarization

Equation (43) can be easily applied in the unpolarized case by setting $z_\uparrow = z_\downarrow$, such that the total density is given by

$$\lambda_T^d n = \lambda_T^d n_0 + 2\sum_{n=2}^\infty n\Delta b_n z^n, \quad (49)$$

where the factor of 2 accounts for the number of species. Our results for Δb_n yield the curves shown in Fig. 6, where they are compared with the QMC results of Ref. [46] and the Luttinger-Ward results of Ref. [47]. The agreement with the QMC data is outstanding. Moreover, for all the couplings in the figure the Padé and Borel resummations substantially extend the region of agreement. With the exception of the
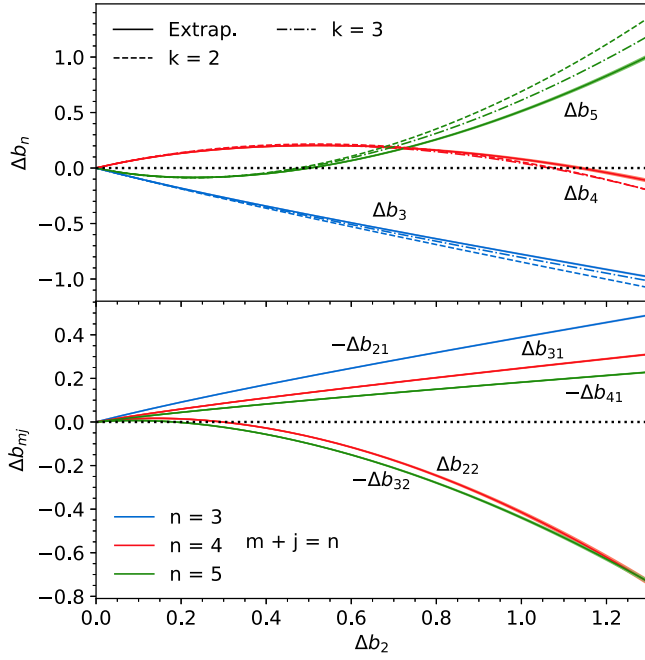
FIG. 5. Weak-coupling zoom-in on Fig. 4, not including the $\exp(-q\beta\epsilon_B)$ factor and plotted as a function of Δb_2. The right edge of the horizontal axis corresponds to $\lambda_2 \simeq 0.588$. The line type, color, and labeling are the same as that of Fig. 1.

weakest coupling in the figure (where the QMC results likely incur volume effects due to the large size of the two-body bound state), the virial expansion is systematically closer to the QMC data than to the Luttinger-Ward results. Although small, this discrepancy remains unresolved.
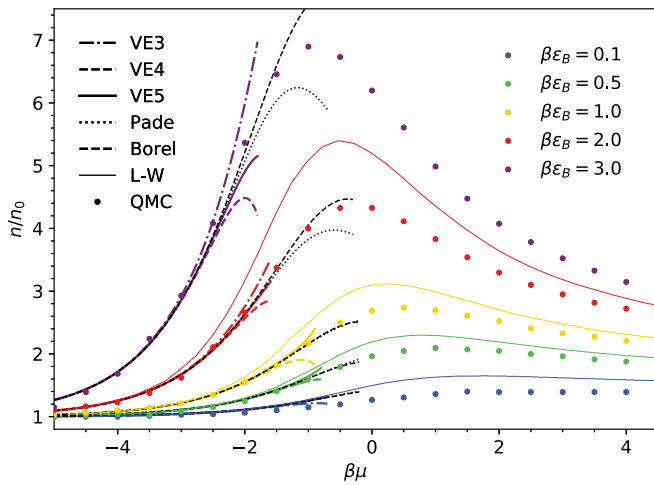
FIG. 6. Density equation of state n, shown in units of the noninteracting counterpart n_0 at different coupling strength $\lambda_2^2 = \beta\epsilon_B$ in two dimensions. The colored dots are the QMC results from Ref. [46], the colored thin line shows the Luttinger-Ward result of Ref. [47], and the colored thick lines are virial expansions at different orders (same line style as in Fig. 2). The black dotted lines and dashed lines are the results, respectively, of Padé and Borel resummation of order [3/2] (see Sec. IV G) using the virial coefficients up to the fifth order.

In Figs. 7 and 8, we compare our results with the experimental data of Refs. [8] and [9], respectively. In all cases, the agreement is remarkable in the regions where the virial expansion is expected to work. Naturally, that region is pushed to progressively more negative $\beta\mu$ as the coupling is increased; in other words, the radius of convergence of the virial expansion decreases as the coupling increases. However, it is also clear that, beyond weak and intermediate couplings (roughly up to $\beta\epsilon_B = 3.0$), the benefits of pushing the virial expansion up to fifth order start to diminish, if the virial expansion is taken at face value. We find, on the other hand, that Padé and Borel resummations dramatically enhance the usefulness of the virial coefficients. As shown in Fig. 7 (left and center panels in particular), our Borel resummations of the virial expansion agree not only qualitatively but in several cases also quantitatively with the experimental data.

2. Contact

In two dimensions, the contact is defined as

$$\mathcal{I} = \frac{2\pi}{\beta} \frac{\partial(\beta\Omega)}{\partial \ln(a_0/\lambda_T)}, \tag{50}$$

such that its virial expansion becomes

$$\mathcal{I} = \frac{(2\pi)^2}{\lambda_T^2} Q_1 \sum_{m=2}^{\infty} c_m z^m, \tag{51}$$

where

$$c_m = \lambda_2 \frac{\partial \Delta b_m}{\partial \lambda_2}. \tag{52}$$

The Beth-Uhlenbeck formula yields

$$c_2 = 2\lambda_2^2 e^{\lambda_2^2} \left[1 + 2 \int_0^\infty dy \frac{y e^{-\lambda_2^2(y^2+1)}}{\pi^2 + 4\ln^2 y} \right], \tag{53}$$

as shown in Refs. [39,46]. Using the λ_2 dependence of our results for Δb_n, we obtained the virial expansion of $\mathcal{I}$ up to fifth order. In Fig. 9 we show the dimensionless, intensive form of the contact, $\mathcal{I}\lambda_T^4/(8\pi^2 L^2)$, as a function of $\beta\mu$ in the virial expansion and compared with the QMC results from Ref. [46]. As with the equation of state shown above, the agreement with the QMC data is remarkable in the region where the virial expansion is expected to work well.

E. Virial coefficients in three dimensions

Finally, in three dimensions we have [20,48]

$$\Delta b_2^{\text{3D,exact}} = \frac{e^{\lambda_3^2}}{\sqrt{2}}[1 + \text{erf}(\lambda_3)], \tag{54}$$

where $\lambda_3 = \sqrt{\beta}/a_0$, and a_0 is the s-wave scattering length. Note the unitary limit corresponds to $\lambda_3 = 0$ and we only explore $\lambda_3 < 0$ regime in this work.

In Figs. 10 and 11, we present our results for Δb_n for the 3D Fermi gas with attractive interactions. These plots parallel the main figure of our previous work of Ref. [18], where we show the same results as a function of Δb_2. For completeness, future reference, and to parallel our discussion
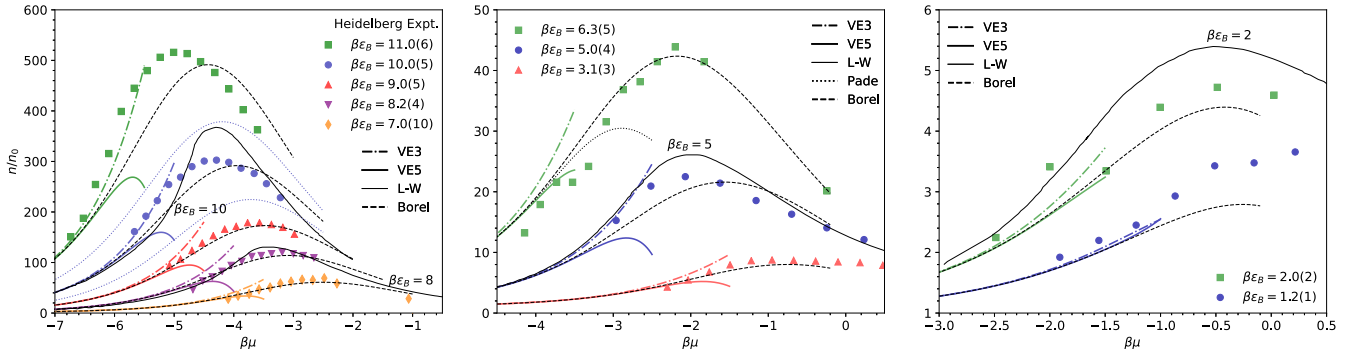
FIG. 7. Density equation of state n of the 2D attractive Fermi gas, shown in units of the noninteracting counterpart n_0 at different coupling strength $\lambda_2^2 = \beta\epsilon_B$ in two dimensions. From bottom to top, the curves and data correspond to $\beta\epsilon_B = 0.1, 0.5, 1.0, 2.0$, and 3.0. The colored symbols are the results of experimental analyses from Ref. [8] and the colored lines show the virial expansion at different orders (following the same line style as in previous figures). (Note: the fourth-order case is omitted from this figure only for clarity.) The black dashed lines are the results of Borel resummation of order [3/2] (see Sec. IV G) using coefficients up to the fifth order. The thin black solid lines are the Luttinger-Ward results of Ref. [47], around which the nearby labels indicate the corresponding $\beta\epsilon_B$. Only the central value of our estimates is used in these plots; the relative error on the virial coefficients from continuous-time extrapolation can reach 15% at the strongest couplings shown in the left panel, although that does not translate into a significant change in the scale shown. Also in the left panel, the blue dotted lines show our Borel-resummed results at $\beta\epsilon_B = 9.5$ (lower) and 10.5 (upper), respectively, which enclose the experimental points completely (in agreement with the experimental uncertainty on $\beta\epsilon_B$). In the middle panel, we also present the [3/2] Padé result as a black dotted line for $\beta\epsilon_B = 6.3$ to demonstrate the performance difference between the two resummation techniques at strong coupling. Reference [8] also provides data at $\beta\epsilon_B = 0.45(5)$, but mostly at large $\beta\mu > 0$ and therefore not shown here.

in lower dimensions, Fig. 10 shows our results as a function of $-1/\lambda_3$ to display the weak-coupling regime, while in Fig. 11 we plot the approach to the unitary limit ($\lambda_3 = 0$) as a function of λ_3. In the latter, we find excellent agreement with the exact Δb_3 of Ref. [49] (see also Refs. [50–53]).

The bottom panels of Fig. 10 and 11 show the subspace decomposition of Δb_n into Δb_{mj}. The qualitative similarities with lower dimensions are clear. Here, however, we have explored a coupling regime in which no two-body bound states are yet formed, such that the introduction of the $\exp(-q\beta\epsilon_B)$ factor is not needed. As the unitary limit is approached, however (see left edge of Fig. 11), all of the coefficients we computed start to display increased curvature. Beyond that point, we expect an exponential increase characterized by $\exp(q\beta\epsilon_B)$ precisely as in lower dimensions. The rapid downturn of Δb_3 at strong coupling was, in fact, already noticed in Ref. [49], while the same feature for Δb_4 appeared in Ref. [53]. Here, we see that that behavior is inevitable as
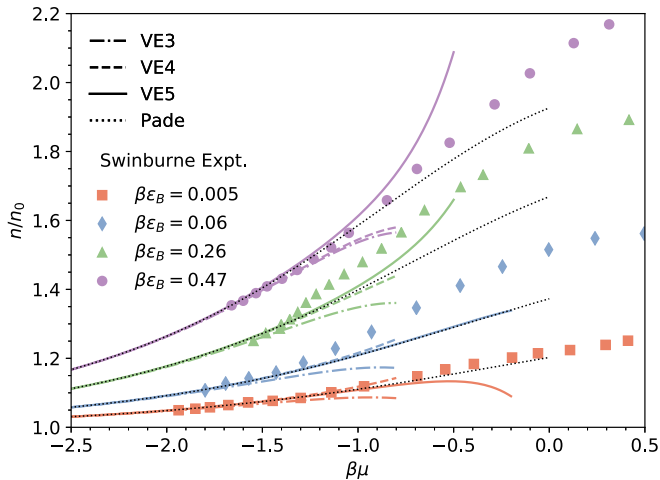

FIG. 8. Density equation of state n, shown in units of the noninteracting counterpart n_0 at different coupling strength $\lambda_2^2 = \beta\epsilon_B$ in two dimensions. The colored symbols are the results of experimental analyses from Ref. [9] and the colored lines are virial expansions at different orders (the same line style applied). The black dotted lines and dashed lines are the results, respectively, of Padé and Borel resummation (see Sec. IV G) of order [3/2] using coefficients up to the fifth order.
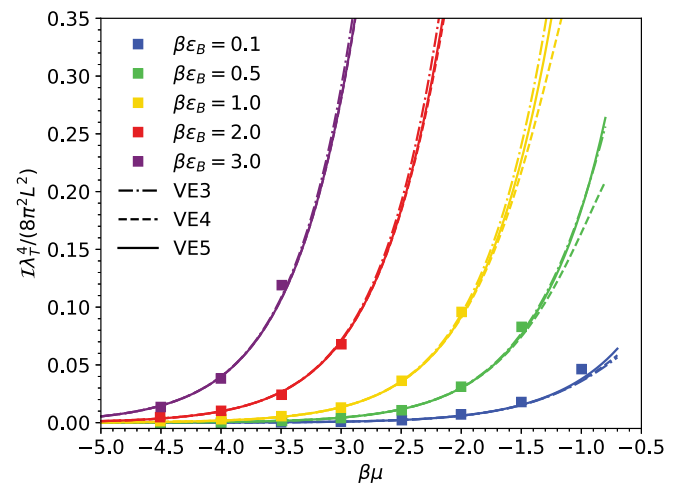

FIG. 9. Contact $\mathcal{I}$, represented in the dimensionless form $\mathcal{I}\lambda_T^4/(8\pi^2 L^2)$, as a function of $\beta\mu$ in two dimensions. The squares are the QMC results of Ref. [46] and the lines are the results of virial expansion at various orders (dash-dotted lines for third order, dashed lines for fourth order, and solid lines for fifth order). From bottom to top, the data shown correspond to coupling strengths $\beta\epsilon_B = 0.1, 0.5, 1.0, 2.0$, and 3.0.
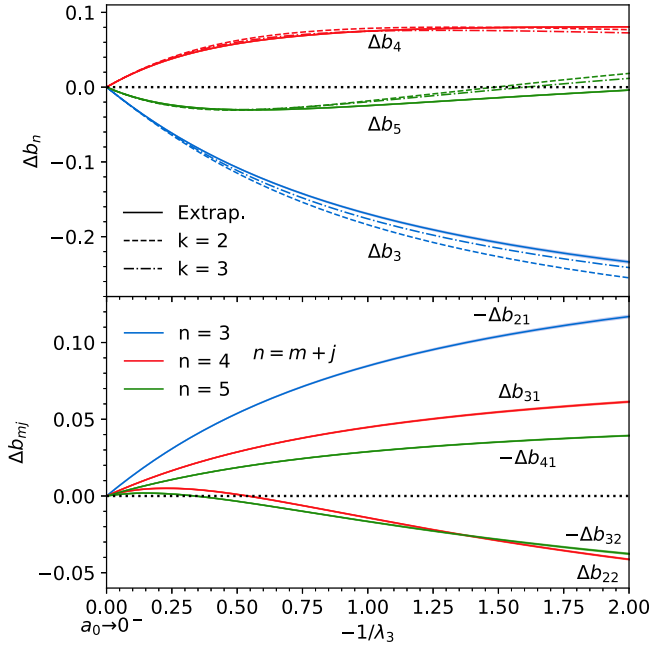
FIG. 10. Δb_n for $n = 3$–5 for the 3D Fermi gas in the weak-coupling regime, as a function of the dimensionless coupling λ_3. The $k = 2$ results are shown with dashed lines, $k = 3$ with dash-dotted lines, and the $k \to \infty$ extrapolation with solid lines. Results for Δb_3 appear in blue, for Δb_4 in red, and for Δb_5 in green, as labeled, following the same convention as Fig. 1.

FIG. 11. Δb_n for $n = 3$–5 for the 3D Fermi gas in the vicinity of the unitary regime ($a_0 \to \infty$, which corresponds to $\lambda_3 = 0$), as a function of the dimensionless coupling λ_3. The exact result for Δb_3 from Ref. [49] appears as a thin solid black line. The $k = 2$ results are shown with dashed lines, $k = 3$ with dash-dotted lines, and the $k \to \infty$ extrapolation with solid lines. Results for Δb_3 appear in blue, for Δb_4 in red, and for Δb_5 in green, following the same convention as Fig. 1.

it is merely a consequence of the dominance of Δb_{m2} (with $m = 2, 3$) over Δb_{m1} (with $m = 3, 4$). However, the sign difference between these terms, as in lower dimensions, results in cancellations that make fully numerical determinations of Δb_4 and Δb_5 a difficult task. Finally, we note that our analysis of Δb_{mj}, and their apparent systematic behavior, suggests that the conjecture of Refs. [54,55] on the high-order virial coefficients in the unitary limit may be refined by focusing on the subspaces rather than the full Δb_n.

F. Applications in three dimensions

1. Density equation of state in the unitary limit

In Fig. 12, we show a comparison of the density equation of state, following closely the format of Fig. 5 of Ref. [58]. By plotting the density relative to the third-order virial expansion, and dividing by z^4, the authors of Ref. [58] showed how their diagrammatic Monte Carlo data compare with previous work on the fourth-order virial coefficient coming from experiments and theory. Our prediction for Δb_5 allows us to take that comparison further (see orange shaded region in Fig. 12), showing excellent agreement with the diagrammatic Monte Carlo results.

In Fig. 13, we present our results for the density equation of state in the unitary limit and compare with the complex-Langevin results of Ref. [59]. The fifth-order expansion shows the best agreement compared to its lower-order counterparts, although the improvement is mostly marginal. When applying the Padé resummation technique, however, the agreement with the data is extended even beyond $\beta\mu =$
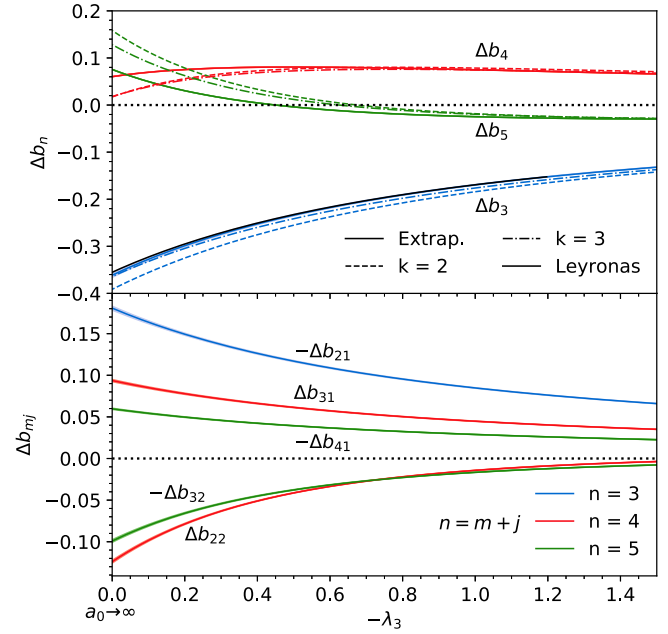
0. Notably, the change in curvature displayed by the data is reproduced by the Padé approximant. Beyond $\beta\mu = 0.6$, however, the Padé approximant progressively departs from the data. The Borel-Padé resummation shows performance very similar to that of pure Padé resummation and is therefore omitted.
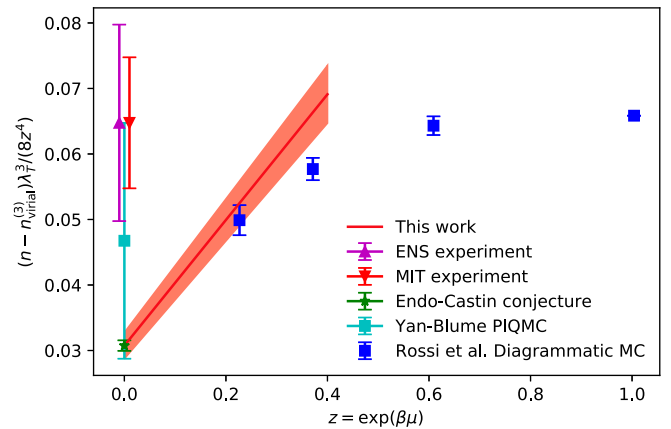

FIG. 12. Density equation of state n of the unitary Fermi gas, relative to the corresponding third-order virial expansion, in units of the thermal wavelength λ_T, as a function of the fugacity z. For comparison, the experimental results of Refs. [6,7] are shown alongside the theoretical predictions of Refs. [56–58] and this work.
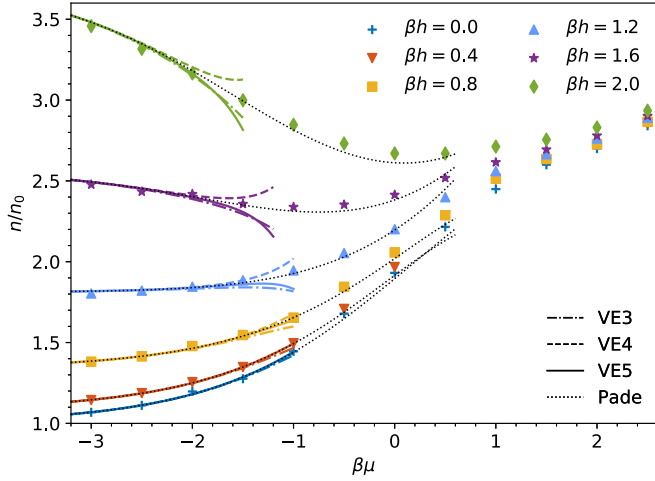
FIG. 13. Density equation of state n of the unitary Fermi gas, shown in units of the noninteracting, unpolarized counterpart n_0, for several values of the chemical potential difference $\beta h = \beta(\mu_\uparrow - \mu_\downarrow)/2$. The colored symbols are complex-Langevin results from Ref. [59] and the colored lines show the virial expansion at various orders: dash-dotted line at third order, dashed line at fourth order, and solid line at fifth order. The black dotted line is the result of the [3/2] Padé resummation (see Sec. IV G). The limiting value for $\beta\mu \to -\infty$ is known exactly and is given by $\cosh(\beta h)$.

2. Compressibility in the unitary limit

The compressibility κ is defined as

$$\kappa = -\frac{1}{V}\left[\frac{\partial V}{\partial P}\right]_T = \frac{\beta}{n^2}\left[\frac{\partial n}{\partial \beta\mu}\right]_T, \tag{55}$$

where, in terms of virial expansion,

$$\frac{\partial n}{\partial(\beta\mu)} = \frac{\partial n_0}{\partial(\beta\mu)} + \sum_{m=2}^{\infty} m^2 \sum_{i+j=m} \Delta b_{ij} z_\uparrow^i z_\downarrow^j. \tag{56}$$

In Fig. 14, we present our estimates for the compressibility κ, shown in units of its noninteracting counterpart $\kappa_0 = 3/(2n\epsilon_F)$, in the unitary limit and compare them with the experimental measurements from Ref. [7], the Luttinger-Ward calculations of Ref. [60], and the complex-Langevin results from Ref. [59].

The results of Padé and Borel-Padé resummations show much better agreement with experimental data than the finite-order virial expansion, even well beyond the region of the virial expansion $z \ll 1$. Specifically, the resummations smoothly follow the trend of the experimental data up to fugacities as large as $z = 10$ (maximum fugacity shown in Fig. 14), which is surprising considering that the superfluid transition occurs at $z \simeq 10$.

3. Tan contact

For completeness, we cite the equations for the contact and its virial expansion, as done above in one and two dimensions. Our results for the contact at unitarity are presented elsewhere [18]. In three dimensions, the contact is defined as

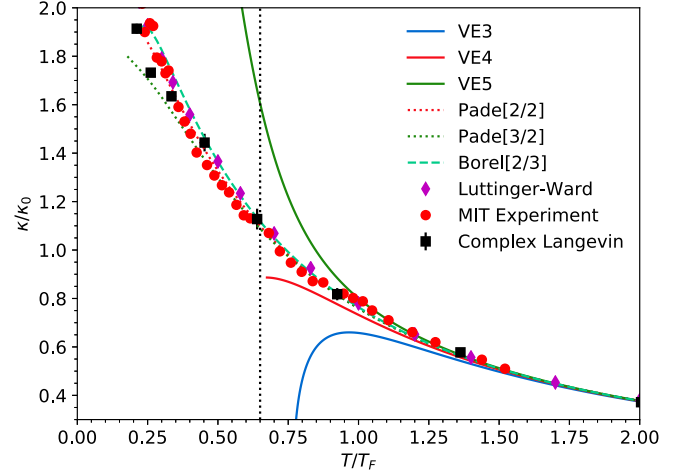$$\mathcal{I} = -\frac{4\pi}{\beta}\frac{\partial(\beta\Omega)}{\partial a_0^{-1}}, \tag{57}$$

FIG. 14. Compressibility κ of the unitary Fermi gas in units of its noninteracting, ground-state counterpart κ_0, as a function of the temperature T in units of the Fermi temperature T_F. Our results for the virial expansion for fugacity $z \in [0, 1]$ are shown as solid lines: blue for third order, red for fourth order, and green for fifth order. The dotted lines are the result of Padé resummation of order [2/2] (red) and [3/2] (green), respectively. The cyan dashed line is the result of a [2/3] Borel-Padé resummation (see Sec. IV G). Other resummation orders are omitted due to the appearance of poles on the real axis in the region of interest. The vertical dotted line corresponds to the approximate T/T_F where $z = 1$ for the three resummed results. The red circles show the data from the MIT experiment of Ref. [7]. The purple diamonds are the Luttinger-Ward calculations of Ref. [60]. The black squares are complex-Langevin results from Ref. [59].

such that its virial expansion reads

$$\mathcal{I} = \frac{8\pi^2}{\lambda_T} Q_1 \sum_{m=2}^{\infty} c_m z^m, \tag{58}$$

where

$$c_m = \frac{1}{\sqrt{2\pi}}\frac{\partial \Delta b_m}{\partial \lambda_3}. \tag{59}$$

The Beth-Uhlenbeck formula yields

$$c_2 = \frac{1}{\pi} + \frac{1}{\sqrt{\pi}}\lambda_3\, e^{\lambda_3^2}(1 + \mathrm{erf}(\lambda_3)). \tag{60}$$

G. Resummation techniques

Before concluding, we present more details on the resummation techniques used in this work, namely, the Padé and Borel-Padé resummations, which we have found useful in extending the applicability of the virial expansion. Generally speaking, the Padé resummation, based on fitting a Padé approximant (see below), is useful when a series is finitely truncated, as in the case of virial expansion. In such cases, the Padé approximant is often better behaved than the partial sums of the original series, and it may even work where the original series diverges, i.e., beyond the radius of convergence of the series. In our case, the technique is simple to apply: the coefficients Δb_n that we calculated determine the unknown coefficients of a Padé approximant which is a rational function $P(z)/Q(z)$, where P and Q are polynomials of degrees a and b,

respectively. Such an approximant is denoted by [a/b]. Using m available virial coefficients, it is possible to fully determine m coefficients in P and Q, which means that $a + b = m$ (note that the independent term in Q is set to 1 by convention). By definition, the Taylor expansion of $P(z)/Q(z)$ at small z reproduces the input virial coefficients.

The Borel-Padé resummation is based on applying a Borel summation [61,62], followed by a Padé fit and reverse (integral) Borel transform (which is a Laplace transform). In short, the Borel summation amounts to replacing each coefficient Δb_n by $\Delta b_n/n!$; the resulting function is fit with a Padé approximant, and that approximant is then numerically integrated to (effectively) undo the introduction of the $n!$ factor. Further details on this well-known technique can be found, for instance, in the Supplemental Material of Ref. [18].

Such an approach has been applied in many other areas (famously in the calculation of critical exponents [63]) ranging from QCD [64] to ultracold atomic physics [65,66]. The method is particularly useful for summing diverging asymptotic series, which is our motivation for using it in two dimensions at strong coupling. We emphasize, however, that there is only indirect evidence that the virial expansion is an asymptotic series in any particular situation (e.g., in one dimensions such evidence is shown in Fig. 2 of Ref. [14]). To the best of our knowledge there is no rigorous proof of this property in any interacting system.

In fact, our empirical observations are that the Borel-Padé resummation yields better qualitative behavior and better overall agreement with experiments at strong coupling than the pure Padé fit mentioned above (see middle panel of Fig. 7). At weak coupling, on the other hand, both techniques yield similar results (see, e.g., Fig. 6). In three dimensions, the strongest *effective* coupling corresponds to the unitary limit; beyond that point the strong attraction leads to the formation of bosonic dimers whose interaction is, as a residual effect, weakly repulsive. However, the two resummation methods still yield similar results at unitarity as the magnitude of the virial coefficients is small. It is only for positive λ_3 (corresponding to deeply bound pairs) that Δb_n will start to grow exponentially, as we saw in one and two dimensions, and in that case the Borel-Padé resummation is expected to offer better estimates.

In Fig. 15, we show in more detail a comparison of Padé and Padé-Borel resummations at different orders, as applied to the density equation of state of the 2D attractive Fermi gas. For all couplings, the pure Padé approach of order [3/2] shows the best agreement with the QMC calculations compared with every other lower-order approximant. (For the [1/4] approximant we have found no solution for the Padé coefficients for the given values of the virial coefficients.) We find that, for $\beta\epsilon_B = 2.0$ and 3.0, the [3/1] approximant encounters poles on the positive z axis at $\beta\mu \approx -2.7$ and -1.7, respectively, which underscores the importance of calculating high-order virial coefficients in order to access a wide range of possible Padé approximants.

Although we found remarkable agreement between our resummations and other results in several examples, these techniques admittedly represent a break from the main *a priori* method we used to obtain the virial coefficients, as Padé and Borel methods have not been rigorously justified here (to the
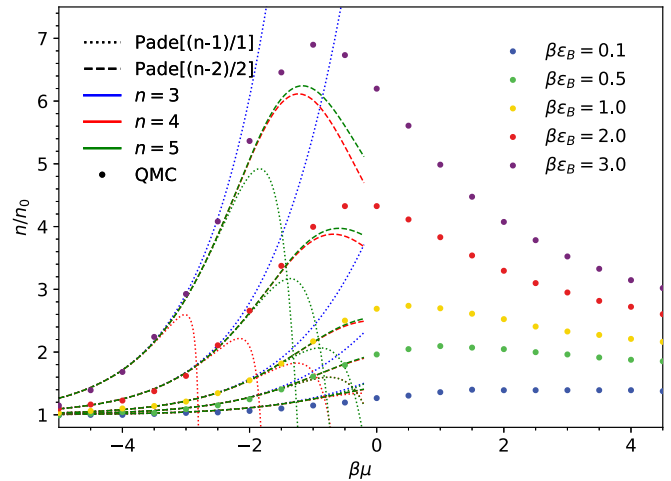

FIG. 15. Density equation of state n, shown in units of the non-interacting counterpart n_0 at different coupling strength $\lambda_2^2 = \beta\epsilon_B$ in two dimensions. The colored dots are the QMC results from Ref. [46], and the colored lines show the results using Padé approximation at different orders. Different colors indicate the higher order of coefficients used in calculating the Padé approximant: blue for $n = 3$, red for $n = 4$, and green for $n = 5$; different line styles represent the degree of denominator in the approximant: dotted line for [$(n-1)/1$] and dashed line for [$(n-2)/2$]. From bottom to top, the data shown correspond to coupling strengths $\beta\epsilon_B = 0.1, 0.5, 1.0, 2.0,$ and 3.0.

best of our knowledge). Future studies may shed light on this matter.

V. SUMMARY AND CONCLUSIONS

In this work we calculated the interaction-induced change in the third to fifth virial coefficients, Δb_3–Δb_5, of spin-1/2 fermions with attractive interactions using a temporal lattice approximation. We provided a few analytic answers in coarse discretizations $k = 1, 2$ before pushing our results to high k ($k = 21$ for Δb_3, $k = 12$ for Δb_4, and $k = 9$ for Δb_5) and extrapolating to the continuous-time limit. Using a renormalization prescription based on matching Δb_2 to the known exact results, we obtained Δb_n for $n = 3, 4, 5$ for a range of attractive couplings in one, two, and three dimensions.

In one dimension, our results for Δb_n agree with previous QMC estimates (obtained at weak coupling) and substantially extend the coupling range. In addition, we obtained the subspace contributions which, as in higher dimensions, appear with similar magnitude but opposite sign, thus partially canceling each other out. We found that the presence of a two-body bound state strongly controls the magnitude of the virial coefficients: multiplying by a factor $\exp(-q\beta\epsilon_B)$, where q is the maximum number of $\uparrow, \downarrow$ pairs and ϵ_B their binding energy, it is possible to show all the virial coefficients we calculated on the same vertical scale.

As an application in one dimension, we compared our results (both partial sums as well as Padé resummation) with complex-Langevin results for the density equation of state at finite polarization, where we found excellent agreement. Similarly, we compared with QMC data for the Tan contact

in the unpolarized case, where we found very good agreement at weak coupling, deteriorating as the coupling is increased (likely due to the limited range of validity of the expansion, but also due to the decreased quality of the data and possible lattice spacing effects at strong coupling).

In two dimensions, the exponential growth mentioned above for one dimension is even more evident: all the coefficients we calculated become very approximately constant once the $\exp(-q\beta\epsilon_B)$ factor is included. The well-known nonperturbative features of this system at weak coupling are smoothly captured by plotting as a function of Δb_2 rather than $\lambda_2^2 = \beta\epsilon_B$. Our results for Δb_3 match very closely those of Ref. [39].

As an application in two dimensions, we compared our results with QMC and experimental data on the density equation of state of the unpolarized system. Partial sums of the virial expansion and resummation results are in excellent agreement with QMC data for a range of negative values of $\beta\mu$, as expected. Furthermore, in all cases the fifth order of the virial expansion yields an improvement over lower orders. Beyond partial sums, the Padé and Padé-Borel resummation shows outstanding agreement in a range of $\beta\mu$ that is substantially larger than that of the partial sums. When comparing with experimental data, the picture is similar: the partial sums give at least reasonable agreement where expected, but it is the Padé-Borel resummation that brings about the most remarkable overall agreement with the data. Finally, our comparison with the Tan contact obtained by QMC methods, where available, shows excellent agreement.

In three dimensions, we calculated Δb_n for couplings up to the unitary limit. Our results for Δb_3 show remarkable agreement with the exact result of Ref. [49] at all couplings. For the unitary limit, our results were discussed at length elsewhere [18]. As no bound states are formed for the couplings we explored in three dimensions, there is no need to include an exponential factor as in the 1D and 2D cases; the growth of the virial coefficients is in fact relatively mild for all the couplings we explored in three dimensions.

As an application in three dimensions, we have calculated the density equation of state at finite chemical potential asymmetry, as well as the compressibility of the unpolarized system. As in the 1D case, we find that the Padé resummation substantially extends the usefulness of the virial expansion. In particular, for the compressibility the agreement with experiments extends as far as $z = 10$.

In one, two, and three dimensions we presented not only Δb_n for $n = 3, 4, 5$, but also the subspace contributions, crucially Δb_{m1} and Δb_{m2}. Discerning these is important because they determine the thermodynamics of the polarized version of the systems we studied. In particular for Δb_4 and Δb_5 the subspace contributions enter with similar magnitudes but opposing signs in all the cases we studied, indicating that the final answers for those coefficients are the result of potentially delicate, coupling-dependent cancellations.

Finally, it should be pointed out that, although we have shown results for a variety of attractively interacting Fermi gases, our analytic results apply to repulsively interacting cases as well. We defer the analysis of the repulsive case to future work. To facilitate the application of our results to those and other cases, we have made our analytic formulas available in a PYTHON code as Supplemental Material [19], along with data tables for the extrapolated virial coefficients.

[1] S. Giorgini, L. P. Pitaevskii, and S. Stringari, Theory of ultracold Fermi gases, Rev. Mod. Phys. **80**, 1215 (2008).

[2] I. Bloch, J. Dalibard, and W. Zwerger, Many-body physics with ultracold gases, Rev. Mod. Phys. **80**, 885 (2008).

[3] *Ultracold Fermi Gases, Proceedings of the International School of Physics "Enrico Fermi"*, Course CLXIV, Varenna, 2006, edited by M. Inguscio, W. Ketterle, and C. Salomon, Vol. 3 (IOS Press, Amsterdam, 2008), Chap. 1, pp. 1–75.

[4] C. Chin, R. Grimm, P. Julienne, and E. Tiesinga, Feshbach resonances in ultracold gases, Rev. Mod. Phys. **82**, 1225 (2010).

[5] M. Lewenstein, A. Sanpera, and V. Ahufinger, *Ultracold Atoms in Optical Lattices: Simulating Quantum Many-Body Systems* (Oxford University Press, New York, 2012).

[6] S. Nascimbene, N. Navon, K. J. Jiang, F. Chevy, and C. Salomon, Exploring the thermodynamics of a universal Fermi gas, Nature (London) **463**, 1057 (2010).

[7] M. J. H. Ku, A. T. Sommer, L. W. Cheuk, and M. W. Zwierlein, Revealing the superfluid lambda transition in the universal thermodynamics of a unitary Fermi gas, Science **335**, 563 (2012).

[8] I. Boettcher, L. Bayha, D. Kedar, P. A. Murthy, M. Neidig, M. G. Ries, A. N. Wenz, G. Zürn, S. Jochim, and T. Enss, Equation of State of Ultracold Fermions in the 2D BEC-BCS Crossover Region, Phys. Rev. Lett. **116**, 045303 (2016).

[9] K. Fenech, P. Dyke, T. Peppler, M. G. Lingham, S. Hoinka, H. Hu, and C. J. Vale, Thermodynamics of an Attractive 2D Fermi Gas, Phys. Rev. Lett. **116**, 045302 (2016).

[10] X.-J. Liu, Virial expansion for a strongly correlated Fermi system and its application to ultracold atomic Fermi gases, Phys. Rep. **524**, 37 (2013).

[11] C. J. Horowitz and A. Schwenk, The virial equation of state of low-density neutron matter, Phys. Lett. B **638**, 153 (2006).

[12] C. J. Horowitz and A. Schwenk, The neutrino response of low-density neutron matter from the virial expansion, Phys. Lett. B **642**, 326 (2006).

[13] C. J. Horowitz and A. Schwenk, Cluster formation and the virial equation of state of low-density nuclear matter, Nucl. Phys. A **776**, 55 (2006).

[14] C. R. Shill and J. E. Drut, Virial coefficients of 1D and 2D Fermi gases by stochastic methods and a semiclassical lattice approximation, Phys. Rev. A **98**, 053615 (2018).

[15] Y. Hou, A. Czejdo, J. DeChant, C. R. Shill, and J. E. Drut, Leading- and next-to-leading-order semiclassical approximation to the first seven virial coefficients of spin-1/2 fermions across spatial dimensions, Phys. Rev. A **100**, 063627 (2019).

[16] K. J. Morrell, C. E. Berger, and J. E. Drut, Third- and fourth-order virial coefficients of harmonically trapped fermions in a semiclassical approximation, Phys. Rev. A **100**, 063626 (2019).

[17] C. E. Berger, K. J. Morrell, and J. E. Drut, Thermodynamics of rotating quantum matter in the virial expansion, Phys. Rev. A **102**, 023309 (2020).

[18] Y. Hou and J. E. Drut, The Fourth- and Fifth-Order Virial Coefficients from Weak Coupling to Unitary, Phys. Rev. Lett **125**, 050403 (2020).

[19] See Supplemental Material at http://link.aps.org/supplemental/10.1103/PhysRevA.102.033319 for PYTHON code and data tables.

[20] E. Beth and G. E. Uhlenbeck, The quantum theory of the non-ideal gas. II. Behaviour at low temperatures, Phys. (Utrecht) **4**, 915 (1937).

[21] M. D. Hoffman, P. D. Javernick, A. C. Loheac, W. J. Porter, E. R. Anderson, and J. E. Drut, Universality in one-dimensional fermions at finite temperature: Density, compressibility, and contact, Phys. Rev. A **91**, 033618 (2015).

[22] A. C. Loheac, J. Braun, and J. E. Drut, Polarized fermions in one dimension: Density and polarization from complex Langevin calculations, perturbation theory, and the virial expansion, Phys. Rev. D **98**, 054507 (2018).

[23] S. Tan, Energetics of a strongly correlated Fermi gas, Ann. Phys. **323**, 2952 (2008).

[24] S. Tan, Large momentum part of a strongly correlated Fermi gas, Ann. Phys. **323**, 2971 (2008).

[25] S. Tan, Generalized virial theorem and pressure relation for a strongly correlated Fermi gas, Ann. Phys. **323**, 2987 (2008).

[26] S. Zhang and A. J. Leggett, Sum-rule analysis of radio-frequency spectroscopy of ultracold Fermi gas, Phys. Rev. A **77**, 033614 (2008).

[27] F. Werner, Virial theorems for trapped cold atoms, Phys. Rev. A **78**, 025601 (2008).

[28] E. Braaten and L. Platter, Exact Relations for a Strongly-Interacting Fermi Gas from the Operator Product Expansion, Phys. Rev. Lett. **100**, 205301 (2008).

[29] E. Braaten, D. Kang, and L. Platter, Universal relations for a strongly interacting Fermi gas near a Feshbach resonance, Phys. Rev. A **78**, 053606 (2008).

[30] E. Braaten, D. Kang, and L. Platter, Short-Time Operator Product Expansion for rf Spectroscopy of a Strongly Interacting Fermi Gas, Phys. Rev. Lett. **104**, 223004 (2010).

[31] D. T. Son and E. G. Thompson, Short-distance and short-time structure of a unitary Fermi gas, Phys. Rev. A **81**, 063634 (2010).

[32] E. Taylor and M. Randeria, Viscosity of strongly interacting quantum fluids: Spectral functions and sum rules, Phys. Rev. A **81**, 053610 (2010).

[33] E. Braaten, in *The BCS-BEC Crossover and the Unitary Fermi Gas*, edited by W. Zwerger (Springer-Verlag, Berlin, 2012).

[34] M. Valiente, N. T. Zinner, and K. Mølmer, Universal relations for the two-dimensional spin-1/2 Fermi gas with contact interactions, Phys. Rev. A **84**, 063626 (2011).

[35] M. Valiente, N. T. Zinner, and K. Mølmer, Universal properties of Fermi gases in arbitrary dimensions, Phys. Rev. A **86**, 043616 (2012).

[36] F. Werner and Y. Castin, General relations for quantum gases in two and three dimensions: Two-component fermions, Phys. Rev. A **86**, 013626 (2012).

[37] J. R. McKenney and J. E. Drut, Fermi-Fermi crossover in the ground state of one-dimensional few-body systems with anomalous three-body interactions, Phys. Rev. A **99**, 013615 (2019).

[38] M. Valiente and V. Pastukhov, Anomalous frequency shifts in a one-dimensional trapped Bose gas, Phys. Rev. A **99**, 053607 (2019).

[39] V. Ngampruetikorn, J. Levinsen, and M. M. Parish, Pair Correlations in the Two-Dimensional Fermi Gas, Phys. Rev. Lett. **111**, 265301 (2013).

[40] J. Levinsen and M. M. Parish, Strongly interacting two-dimensional Fermi gases, Annu. Rev. Cold At. Mol. 1 (2015).

[41] X.-J. Liu, H. Hu, and P. D. Drummond, Exact few-body results for strongly correlated quantum gases in two dimensions, Phys. Rev. B **82**, 054524 (2010).

[42] C. Chaffin and T. Schäfer, Scale breaking and fluid dynamics in a dilute two-dimensional Fermi gas, Phys. Rev. A **88**, 043636 (2013).

[43] M. Barth and J. Hofmann, Pairing effects in the nondegenerate limit of the two-dimensional Fermi gas, Phys. Rev. A. **89**, 013614 (2014).

[44] C. R. Ordoñez, Path-integral Fujikawa approach to anomalous virial theorems and equations of state for systems with SO(2, 1) symmetry, Physica **446**, 64 (2016).

[45] W. S. Daza, J. E. Drut, C. L. Lin, and C. R. Ordóñez, Virial expansion for the Tan contact and Beth-Uhlenbeck formula from two-dimensional SO(2, 1) anomalies, Phys. Rev. A **97**, 033630 (2018).

[46] E. R. Anderson and J. E. Drut, Pressure, Compressibility, and Contact of the Two-Dimensional Attractive Fermi Gas, Phys. Rev. Lett. **115**, 115301 (2015).

[47] M. Bauer, M. M. Parish, and T. Enss, Universal Equation of State and Pseudogap in the Two-Dimensional Fermi Gas, Phys. Rev. Lett. **112**, 135302 (2014).

[48] D. Lee and T. Schäfer, Cold dilute neutron matter on the lattice. I. Lattice virial coefficients and large scattering lengths, Phys. Rev. C **73**, 015201 (2006).

[49] X. Leyronas, Virial expansion with Feynman diagrams, Phys. Rev. A **84**, 053633 (2011).

[50] X.-J. Liu, H. Hu, and P. D. Drummond, Virial Expansion for a Strongly Correlated Fermi Gas, Phys. Rev. Lett. **102**, 160401 (2009).

[51] D. B. Kaplan and S. Sun, A New Field Theoretic Method for the Virial Expansion, Phys. Rev. Lett. **107**, 030601 (2011).

[52] D. Rakshit, K. M. Daily, and D. Blume, Natural and unnatural parity states of small trapped equal-mass two-component Fermi gases at unitarity and fourth-order virial coefficient, Phys. Rev. A **85**, 033634 (2012).

[53] V. Ngampruetikorn, M. M. Parish, and J. Levinsen, High-temperature limit of the resonant Fermi gas, Phys. Rev. A **91**, 013606 (2015).

[54] R. K. Bhaduri, W. van Dijk, and M. V. N. Murthy, Universal Equation of State of a Unitary Fermionic Gas, Phys. Rev. Lett. **108**, 260402 (2012).

[55] R. K. Bhaduri, W. van Dijk, and M. V. N. Murthy, Higher virial coefficients of a unitary Fermi gas, Phys. Rev. A **88**, 045602 (2013).

[56] Y. Yan and D. Blume, Path Integral Monte Carlo Determination of the Fourth-Order Virial Coefficient for Unitary Two-Component Fermi Gas with Zero-Range Interactions, Phys. Rev. Lett. **116**, 230401 (2016).

[57] S. Endo and Y. Castin, Absence of a four-body Efimov effect in the 2 + 2 fermionic problem, Phys. Rev. A **92**, 053624 (2015).

[58] R. Rossi, T. Ohgoe, K. Van Houcke, and F. Werner, Resummation of Diagrammatic Series with Zero Convergence Radius

for Strongly Correlated Fermions, Phys. Rev. Lett. **121**, 130405 (2018).

[59] L. Rammelmüller, A. C. Loheac, J. E. Drut, and J. Braun, Finite-Temperature Equation of State of Polarized Fermions at Unitarity, Phys. Rev. Lett. **121**, 173001 (2018).

[60] T. Enss and R. Haussmann, Quantum Mechanical Limitations to Spin Diffusion in the Unitary Fermi Gas, Phys. Rev. Lett. **109**, 195303 (2012).

[61] E. Brézin, J. C. Le Guillou, and J. Zinn-Justin, Perturbation theory at large order. I. The ϕ^{2n} interaction, Phys. Rev. D **15**, 1544 (1977).

[62] C. M. Bender and C. Heissenberg, Convergent and divergent series in physics, arXiv:1703.05164.

[63] R. Guida and J. Zinn-Justin, Critical exponents of the N vector model, J. Phys. A **31**, 8103 (1998).

[64] M. Pindor, Padé approximants and Borel summation for QCD perturbation expansions, arXiv:hep-th/9903151.

[65] Y. Nishida and D. T. Son, ϵ Expansion for a Fermi Gas at Infinite Scattering Length, Phys. Rev. Lett. **97**, 050403 (2006).

[66] P. Arnold, J. E. Drut, and D. T. Son, Next-to-next-to-leading-order ϵ expansion for a Fermi gas at infinite scattering length, Phys. Rev. A **75**, 043605 (2007).